Level structure above the 17^+ isomeric state in $^{152}_{69}Tm_{83}$

B. S. Nara Singh,[1,*] D. M. Cullen,[1] M. J. Taylor,[1,2] P. C. Srivastava,[3,4] P. Van Isacker,[3] O. Beeke,[1] B. Dodson,[1] C. Scholey,[5] D. O'Donell,[6] U. Jakobson,[5,7] T. Grahn,[5] P. T. Greenlees,[5] P. M. Jones,[5,8] R. Julin,[5] S. Khan,[1] M. Leino,[5] A.-P. Leppänen,[5,9] S. Eeckhaudt,[5] K. Mäntyniemi,[5] J. Pakarinen,[5] P. Peura,[5,10] P. Rahkila,[5] J. Sarén,[5] J. Sorri,[5,11] J. Uusitalo,[5] and M. Venhart[12]

[1]*Schuster Building, School of Physics and Astronomy, The University of Manchester, Manchester M13 9PL, United Kingdom*

[2]*Division of Cancer Sciences, The Univserity of Manchester, Manchester M13 9PL, United Kingdom*

[3]*Grand Accélérateur National d'Ions Lourds, CEA/DRF-CNRS/IN2P3, Boulevard Henri Becquerel, F-14076 Caen, France*

[4]*Department of Physics, Indian Institute of Technology Roorkee, Roorkee 247 667, India*

[5]*University of Jyvaskyla, Department of Physics, P.O. Box 35, FI-40014 University of Jyvaskyla, Finland*

[6]*School of Computing, Engineering and Physical Sciences, University of the West of Scotland, Paisley, PA1 2BE, United Kingdom*

[7]*Department of Chemistry-Radiochemistry, P.O. Box 55, FI-00014 University of Helsinki, Finland*

[8]*Department of Nuclear Physics, iThemba Laboratory for Accelerator Based Sciences, P.O. Box 722, Somerset West 7129, South Africa*

[9]*STUK, Radiation and Nuclear Safety Authority, Finland*

[10]*Helsinki Institute of Physics, FI-00014, University of Helsinki, Finland*

[11]*University of Oulu, Sodankylä Geophysical Observatory, Tähteläntie 62, FI-99600 Sodankylä, Finland*

[12]*Institute of Physics, Slovak Academy of Sciences, Dúbravská cesta 9, 845 11 Bratislava, Slovakia*

(Received 6 April 2018; published 28 August 2018)

Excited states above the 17^+ isomeric state in the proton-rich nucleus ^{152}Tm were established by employing the recoil-isomer tagging technique. Data were collected using the JUROGAM gamma-ray array and the GREAT spectrometer together with the recoil ion transport unit (RITU) gas-filled recoil separator and analyzed to identify the prompt and delayed γ decays from the levels in ^{152}Tm. Shell-model calculations, either in a large valence space or in a reduced model space with five protons in the $\pi 0h_{11/2}$ orbital and one neutron in the $\nu 1f_{7/2}$ orbital, agree with the observed energies of the yrast levels up to angular momentum $J = 21$. The observation of near degeneracies in the energy spectrum can be attributed to specific components of the proton-neutron interaction. The isomeric decay of the 17^+ level is not reproduced in the shell-model calculations as it arises from a delicate balance between hindrance due to seniority selection rules and enhancement due to configuration mixing.

DOI: 10.1103/PhysRevC.98.024319

I. INTRODUCTION

The substantial evidence for a subshell gap at proton number $Z = 64$ [1] triggered a great deal of work on proton-rich nuclei in the $A \approx 150$ mass region [2–7]. The similarities between the doubly magic nuclei ^{146}Gd and ^{208}Pb [1] and the expected influence of the proton-neutron interaction on structural features as observed in the ^{100}Sn region [3,8–10] also fueled further interest. As a result, a wealth of nuclear structure data has become available. This allowed a study of the evolution of level energies and transition strengths in nuclei with a few valence particles outside the ^{146}Gd core. A comparison with the calculations using empirical interactions revealed the crucial roles of the nucleon occupation of the $\pi 0h_{11/2}$ orbital. The interaction between protons in the $\pi 0h_{11/2}$ orbital and neutrons in the $\nu 0h_{9/2}$ orbital is also expected to influence the level structures exhibited by nuclei in this region [4]. As protons are added above the $Z = 64$ subshell closure or neutrons above the $N = 82$ shell closure, the proton-neutron interaction is expected to strengthen and have an effect on the nuclear structure features. For example, differences between the level structures below the 17^+ isomeric states in ^{150}Ho and ^{152}Tm isotones have been provisionally interpreted to arise from the strong influence of the $\pi 0h_{11/2}$-$\nu 0h_{9/2}$ interaction; however, that needs confirmation [4].

The assumption of a doubly magic ^{146}Gd core greatly facilitates shell-model calculations. Consequently, theoretical interpretations of the levels in nuclei with $Z \sim 64$ and $N \sim 82$ are currently feasible. In particular, if one assumes that only protons in the $\pi 0h_{11/2}$ orbital and neutrons in the $\nu 1f_{7/2}$ orbital are active, then the shell-model calculations can be performed relatively easily and a comparison with data can be used to refine or develop nuclear structure models [2,4,5]. The overall aim of such studies is to test models with particular components of the nucleon-nucleon interaction. In an empirical approach, this interaction is extracted from the data or taken from systematics [2,4,5]. For example, experimental knowledge of the structure of $^{148}_{65}Tb_{83}$ [6] determines the $\pi 0h_{11/2}$-$\nu 1f_{7/2}$ interaction or that of $^{146}_{63}Eu_{83}$ [7] fixes the $(\pi 0h_{11/2})^{-1}$-$\nu 1f_{7/2}$ interaction. In contrast, modern shell-model calculations can be performed by utilizing a nucleon-nucleon interaction derived from first principles. Therefore, it is of principal interest to make a comparison between calculations performed using empirical and microscopic interactions to refine our knowledge

*Present address: School of Computing, Engineering and Physical Sciences, University of the West of Scotland, Paisley, PA1 2BE, United Kingdom.

of the latter and to produce better theoretical predictions. In the context of the present work, a comparison between the calculations and experimental data on the levels in $^{152}_{69}Tm_{73}$ can be made to understand the role of the proton-neutron interaction [4].

The nucleus $^{152}_{69}Tm_{83}$ has five protons beyond $Z = 64$ (mainly in the $\pi 0h_{11/2}$ orbital) and one neutron beyond $N = 82$ (mainly in the $\nu 1f_{7/2}$ orbital). Because of the presence of these isolated and low-lying high-j orbitals, the nucleus displays two isomeric states with half-lives ($T_{1/2}$) of 294(12) ns and 42(5) ns that were observed in Ref. [4]. The shorter-lived isomeric state was predicted to be located around 6.3 MeV; however, the excitation energy of this level could not be determined using the data. The levels populated by the decay of the longer lived state were studied previously, which led to a spin and parity assignment of $J^\pi = 17^+$ for the isomeric state. The isomeric nature of this state (and others like it in the region) can be explained with seniority arguments or, equivalently, arguments based on the number of broken nucleon pairs [2]. These studies also led to the conclusion that the levels above the 17^+ isomeric state had a different seniority structure as they involve the breaking of an additional proton pair. In Ref. [4], 12 γ-ray transitions following the decay of the 42 ns isomeric state have been listed. However, no level scheme between the two isomeric states is known to date. In the present work, we performed a recoil-isomer tagging study of ^{152}Tm together with the triple prompt γ-ray coincidence analysis to obtain excited states above the 17^+ isomeric state. The data have been compared with the large-scale shell-model calculations in order to investigate the influence of the proton-neutron interaction on the nuclear structure in ^{152}Tm.

II. EXPERIMENTAL DETAILS

The experiment was carried out for 40 h at the Accelerator Laboratory of the University of Jyväskylä. A $^{64}Zn^{12+}$ beam with an intensity of $\sim$5 pnA was accelerated to an energy of 280 MeV by the K130 cyclotron and was used to bombard a ^{92}Mo target with a thickness of 500 μg/cm^2. Excited states in ^{152}Tm were populated in the ^{92}Mo (^{64}Zn, $3pn$) fusion-evaporation reaction. Prompt γ rays were detected at the target position by the JUROGAM array, which comprised 43 Compton-suppressed high-purity germanium detectors, with a total photopeak efficiency of 4.2% at 1.33 MeV [11]. The evaporation residues were separated from the unreacted beam by the Recoil Ion Transport Unit (RITU) separator [12,13] and were implanted into an aluminium stopper foil at the focal plane where the Gamma-Recoil-Electron-Alpha-Tagging (GREAT) spectrometer was located [14]. These recoiling nuclei were identified on the basis of energy loss and time of flight (ToF) as they passed through a dual multiwire proportional counter (MWPC) system at the entrance of GREAT. In the standard setup, rates of recoil implantations into the double sided silicon strip detector (DSSSD) are limited in order to minimize any damage to the detector. Replacement of the DSSSD with a metal foil in the present dual-MWPC setup lifted such constraints arising from a silicon detector and allowed a higher beam intensity. The planar Ge strip detector in GREAT was placed $\sim$10 mm behind the Al stopper foil to record low-energy delayed γ rays. In order to detect higher energy (>300 keV) γ rays with a better efficiency compared to that of the planar detector, two phase 1 germanium detectors detectors [11] and a segmented clover Ge detector (collectively referred to as the focal-plane Ge, FPGe) were placed surrounding the planar Ge detector [14].

All registered detector signals were time stamped using a 100-MHz clock in the total data readout (TDR) acquisition system [15]. The FPGe detectors were used to detect the energies and timing of γ-ray events that had been delayed (E^D_γ) with respect to the observed prompt γ rays (E^P_γ) at the target position. The GRAIN software package [16] was used to perform offline data sorting and to obtain a three-dimensional E_γ-E_γ-E_γ energy cube as well as two-dimensional E_γ-E_γ energy versus energy and E_γ-T_γ energy versus time matrices. Here, T_γ corresponds to the time difference between a recoil implantation and a delayed γ-ray detection. The events in these histograms were gated by the ToF and the energy-loss signals for the recoils from the dual-MWPC setup. The two dimensional E^D_γ-E^D_γ and E^P_γ-E^P_γ matrices containing delayed-delayed and prompt-prompt coincidence events, respectively, were prepared with a time window of 100 ns. In addition, E^P_γ-E^D_γ prompt-delayed coincidence matrices were also prepared. A condition was imposed which demanded that the decay events at the focal plane were in time correlation with the implanted recoils within a window of 1 μs, corresponding to approximately three times the half-life of the 17^+ isomeric state in ^{152}Tm. For the purpose of background subtraction, matrixes were also prepared with a time window of 1 to 2 μs following the recoil implantation. Background-subtracted histograms were used to perform standard prompt-prompt and prompt-delayed coincidence analysis using the RADWARE [17] package. Furthermore, an E^D_γ-T^D_γ matrix was also constructed in order to obtain the lifetime of the 17^+ isomeric state.

III. RESULTS

The excited states with spins up to 27^+ were observed by identifying γ-ray transitions in ^{152}Tm. Figure 1 shows the deduced level scheme. The known lifetime of the 17^+ isomeric state and the delayed level structure populated by it were also confirmed [4]. Details of the analysis used for obtaining these results are discussed in the following subsections.

A. Decay of the known 17^+ isomeric state

Figure 2(a) shows the focal-plane γ-ray energy spectrum that was obtained by taking a total time projection of the E^D_γ-T^D_γ matrix. The prompt γ-ray transitions between the levels populated by the decay of the 17^+ isomeric state in ^{152}Tm can be seen. However, this spectrum is clearly dominated by the contaminant γ rays from ^{150}Er, ^{151}Tm, and ^{153}Yb nuclei that were produced with higher cross sections when compared to ^{152}Tm. These contaminants are eliminated in Fig. 2(b) by demanding $T^D_\gamma < 1$ μs while the γ-ray transitions below the 17^+ isomeric state in ^{152}Tm are enhanced. The combined time distribution of these γ-ray peaks marked with asterisks in Fig. 2(b) was projected from the E^D_γ-T^D_γ matrix and is shown in Fig. 3. An exponential decay (solid) curve with a constant

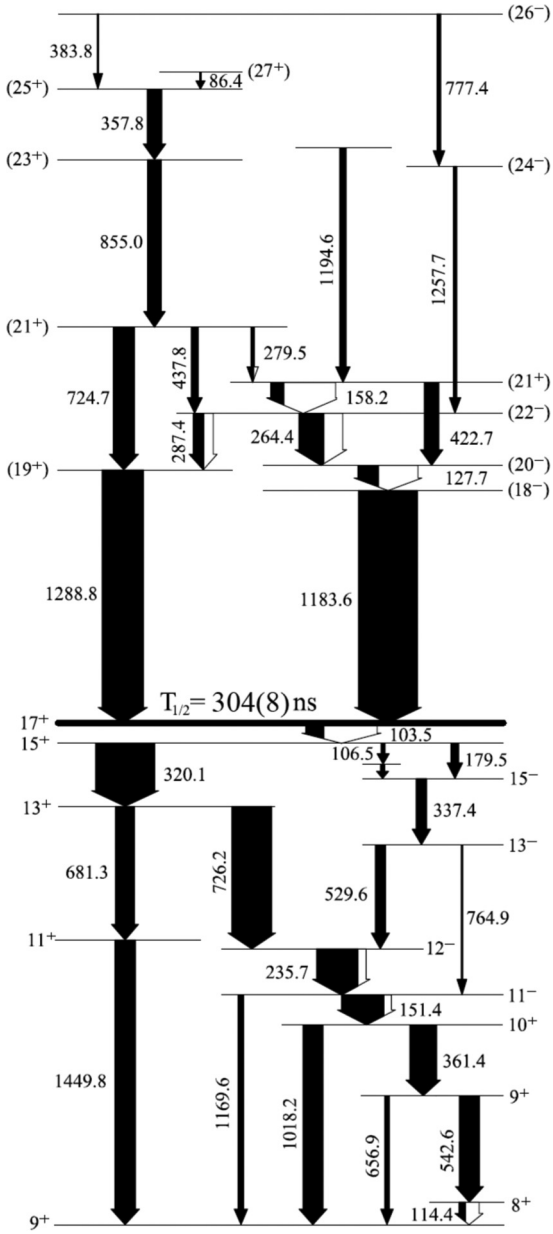

FIG. 1. The deduced level scheme for ^{152}Tm, including the newly observed levels above the known 17^+ isomeric state. Arrow widths are proportional to relative intensity, and unshaded portions represent the amount of internal conversion. The known level scheme below the 17^+ isomeric state [4] is confirmed from an analysis of the focal-plane data. See the text for more details.

background, $f(x) = A\ \exp[-B(x-0.64)] + C$, was fit to this distribution with a χ^2 value of ∼14 in order to obtain a half-life of $T_{1/2} = 304(8)$ ns for the isomeric state. This is consistent with but slightly more accurate than the previously known value of 294(12) ns [4].

A $\gamma\gamma$ coincidence analysis was performed for the delayed γ rays by utilizing the E_γ^D-E_γ^D matrix. The statistics in these delayed spectra are lower compared to that from the previous work [4]. Nevertheless, the known level scheme below the 17^+ isomeric state could be confirmed, except for the nonobservation of the 73-keV transition essentially due to the electron conversion process [4]. Figure 4 shows the delayed γ-ray energy spectra. These spectra were projected from the E_γ^P-E_γ^D matrix by gating on the obtained prompt γ-ray transitions, with energies of 128, 158, 264, 287, 358, 423, 438, 725, 855, 1184, and 1289-keV, populating the isomeric state (see Fig. 1 and Sec. III B). Table I gives the intensities of the delayed γ rays, which were obtained from Fig. 4. As the 765- and 1170-keV γ-ray transitions were not observed in these gated spectra, their intensities (marked with asterisks in Table I) were obtained by using the delayed γ-ray spectrum with no condition on the prompt γ-ray detection. This was possible due to the absence of any contamination in the corresponding γ-ray peaks. The

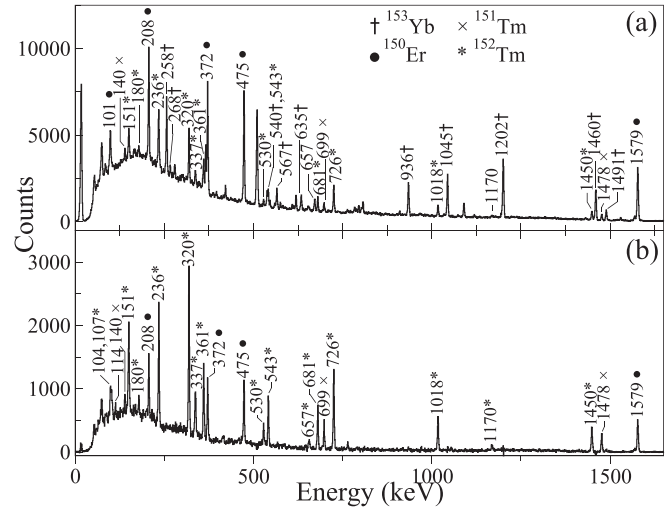

FIG. 2. Focal-plane germanium energy spectra projected from the E_γ^D-T_γ^D matrix with (a) no time condition and (b) a time condition of $T_\gamma^D < 1\ \mu$s displaying relative enhancement of the γ rays belonging to ^{152}Tm (see the text for details).

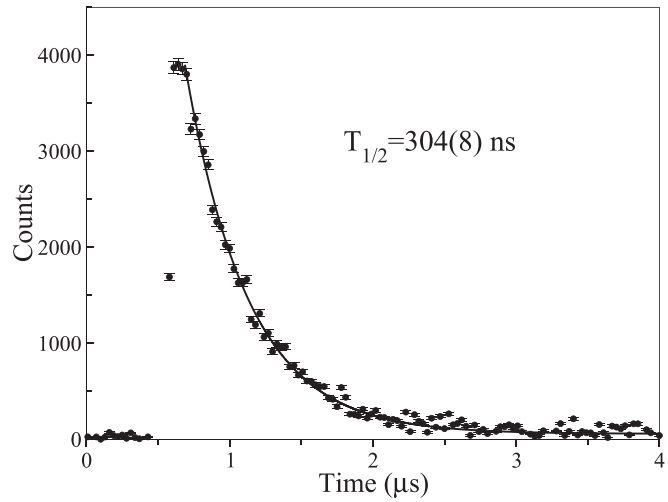

FIG. 3. The time distribution of the γ rays that are marked with asterisks in Fig. 2(b), following the decay of the 17^+ isomeric state in ^{152}Tm. The solid line is an exponential fit to the data in the range between 0.8 and 2.8 μs.

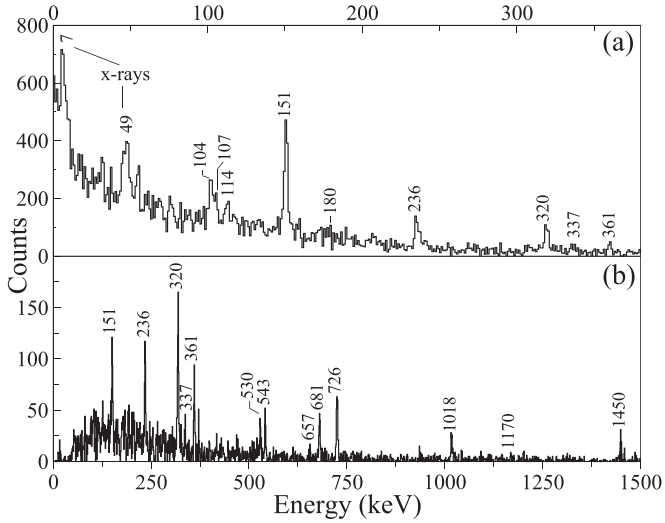

FIG. 4. Delayed γ-ray spectra measured by (a) the planar and (b) focal-plane Ge detectors with a time condition that the events should be recorded within 1 μs after the fusion evaporation reaction and in coincidence with the newly observed prompt γ-ray transitions in ^{152}Tm with energies of 128, 158, 264, 287, 358, 423, 439, 725, 855, 1184, and 1289 keV.

total conversion coefficients for the low-energy transitions, namely, $\alpha_{104} = 5.5 \pm 1.0$ (2.64(11) from BRICC [18]), $\alpha_{114} = 1.6 \pm 0.6$ [2.13(7)], $\alpha_{151} < 0.1$ [0.1102(25)], $\alpha_{236} = 0.41 \pm 0.13$ [0.278(5)], and $\alpha_{320} = 0.064 \pm 0.20$ [0.059(1)] were obtained by analyzing the associated γ-ray intensities. These

TABLE I. Intensities of the delayed γ rays, following the decay of the 17^+ isomeric state with $T_{1/2} = 304(8)$ ns in ^{152}Tm, obtained from spectra shown in Fig. 4. Intensities marked with asterisks were obtained without any condition on the prompt γ-ray detection. See the text for more details.

Energy (keV)	Intensity	
E_γ	This study	Ref. [4]
103.5(1)	23(3)	31(3)
106.5(2)	11(3)	7(1)
114.4(1)	12(2)	11(1)
151.4(1)	81(4)	72(6)
179.5(5)	12(1)	13(1)
235.7(1)	73(4)	70(4)
320.1(1)	100(6)	100(5)
337.4(1)	19(3)	18(1)
361.4(1)	42(4)	45(2)
529.6(1)	25(4)	17(1)
542.6(1)	32(4)	34(2)
656.9(2)	11(3)	8(1)
681.3(1)	45(5)	32(2)
726.2(1)	78(7)	67(5)
764.9(3)	4(1)*	3(1)
1018.2(1)	39(5)	34(2)
1169.8(3)	9(1)*	9(1)
1449.8(2)	44(6)	35(3)

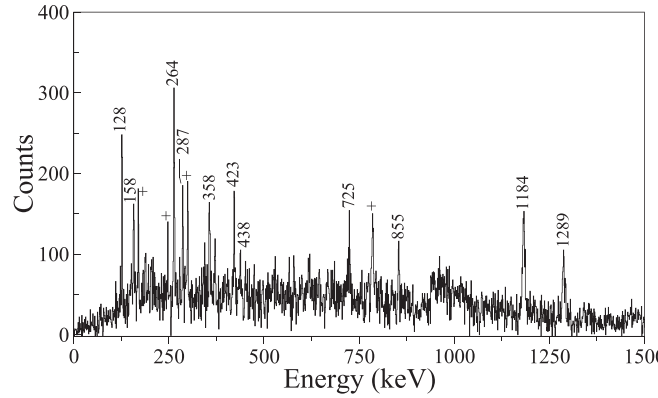

FIG. 5. A γ-ray spectrum measured at the target position and gated by a set of delayed transitions below the 17^+ isomeric state in ^{152}Tm with a half-life of 304(8) ns (see the text for details). The prompt γ decays from the levels above the isomeric state are labeled with their energies. The peaks marked with plus (+) symbols indicate either contamination from ^{150}Er or the prompt γ rays that could not associated with ^{152}Tm.

results and the level scheme below the 17^+ isomeric state from the present work are fully consistent with those from Ref. [4]. Furthermore, a rather good agreement between the experimental data and the large-scale shell-model calculations (see below) supports the spin and parity assignments of the energy levels.

B. Prompt level scheme populating the 17^+ isomeric state

A prompt-delayed $\gamma\gamma$ coincidence analysis was performed by using the E_γ^P-E_γ^D matrix to search for such γ decays at the target position. Figure 5 shows a prompt γ-ray spectrum that was projected by gating on the known delayed γ rays, namely, those with energies of 104, 114, 151, 180, 236, 320, 337, 361 (detected in both the planar and focal-plane Ge detectors), 530, 543, 657, 681, 726, 765, 1018, 1170, and 1450 keV (detected in the focal-plane Ge detectors alone). This coincidence spectrum allowed a clean identification of 17 prompt γ rays in ^{152}Tm and was used to obtain their intensities that are given in Table II. For the transitions marked with daggers (†) in the table, no significant peaks can be seen in Fig. 5. Therefore, the corresponding intensities were obtained from the γ-ray energy spectra projected from the E_γ^P-E_γ^P-E_γ^P energy cube by gating on one or two other relevant γ rays in ^{152}Tm. In this case, no condition of time correlation was imposed between the prompt γ-ray events in the energy cube and the delayed γ-ray events at the focal plane.

Figure 6 shows a few $\gamma\gamma\gamma$ coincidence spectra that were obtained from the E_γ^P-E_γ^P-E_γ^P energy cube. Such spectra were analyzed in order to construct a level scheme corresponding to the prompt γ rays in ^{152}Tm (cf. Fig. 5). The cascade of the 384-, 358-, 855-, 725-, and 1289-keV γ rays in Fig. 1 is supported by the spectrum shown in Fig. 6(a), which was prepared by gating on the 725- and 855-keV γ rays. The 86-keV transition was placed in a parallel branch since it was not found to be in coincidence with the 384-keV transition. The order of the 358- and 855-keV γ rays could not be completely fixed by

TABLE II. Energies, intensities, and initial- and final-state spins and parities for the prompt γ-ray transitions above the $J^\pi = 17^+$ isomeric state in ^{152}Tm with $T_{1/2} = 304(8)$ ns (see the text for more details).

E_γ (keV)	I_γ (Rel %)	$J_i^\pi \rightarrow J_f^\pi$
86.4(1)	2(1)	$(27^+)\rightarrow(25^+)$
127.7(1)	35(3)	$(20^-)\rightarrow(18^-)$
158.2(1)	23(2)	$(21^+)\rightarrow(22^-)$
264.4(1)	42(3)	$(22^-)\rightarrow(20^-)$
279.5(1)	5(1)	$(21^+)\rightarrow(21^+)$
287.4(1)	18(2)	$(22^-)\rightarrow(19^+)$
357.8(1)	25(2)	$(25^+)\rightarrow(23^+)$
383.8(2)	2(1)†	$(24^-)\rightarrow(25^+)$
422.7(1)	25(2)	$(22^-)\rightarrow(20^-)$
437.8(2)	12(2)	$(21^+)\rightarrow(20^-)$
724.7(1)	36(4)	$(21^+)\rightarrow(19^+)$
777.4(2)	6(3)†	$(22^-)\rightarrow(20^-)$
855.0(2)	23(3)	$(23^+)\rightarrow(21^+)$
1183.6(1)	100(4)	$(18^-)\rightarrow(17^+)$
1194.6(5)	11(6)†	$()\rightarrow(21^+)$
1257.7(5)	6(3)†	$(24^-)\rightarrow(22^-)$
1288.8(2)	70(5)	$(19^+)\rightarrow(17^+)$

the observed intensities and, therefore, is tentative. Figure 6(b) was used to place a parallel branch involving the 287- and 438-keV decays that was found not to be in coincidence with the 725-keV transition. The ordering of these two γ rays was fixed by the presence of the 158-keV line and the observed coincidence with the 1195-keV transition. Another parallel branch to the 439-keV decay, involving the 280- and 158-keV

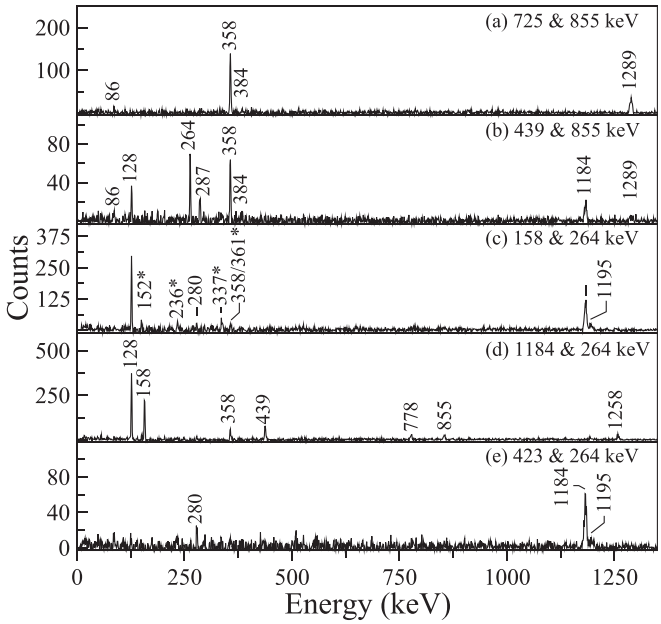

FIG. 6. A collection of prompt γ-ray triple coincidence spectra for the transitions in ^{152}Tm, double-gated with (a) 725- and 855-keV, (b) 438- and 855-keV, (c) 158- and 264-keV, (d) 1184- and 264-keV, and (e) 423- and 264-keV γ-ray transitions.

transitions, was established using Fig. 6(c). This spectrum also supported the placement of the 128- and 1184-keV transitions that have different decay paths to the isomeric state when compared to that of the 1289-keV transition. Finally, Figs. 6(d) and 6(e) were used to place the 423-, 777-, and 1258-keV transitions as shown in Fig. 1. Several peaks marked with asterisks (*) were observed in Fig. 6(c), corresponding to the γ-ray transitions below the 17^+ isomeric state (cf. Fig. 1). Such events are not expected in this triple coincident spectra detected by JUROGAM, if they are originating only from the decay of the 17^+ isomeric state. Presence of these events at the target position indicates that either there is an unobserved transition bypassing the 17^+ isomeric state or the in-flight decays of this isomeric state with $T_{1/2} = 304(8)$ ns in ^{152}Tm recoil nuclei.

The spin and parities, J^π, of levels shown in Fig. 1 above the 17^+ isomeric state could only be assigned tentatively in this work. The observed γ-ray intensities and internal conversion coefficients as well as γ-ray coincidence analyses and level energies were used for this purpose. These assignments were further supported by our large-scale shell-model calculations (see below). The unshaded arrow widths in the level scheme represent electron conversion for the low-energy γ rays. The values of $\alpha_{128} = 1.9 \pm 0.3$. (1.23(4) from BRICC [18]) and $\alpha_{158} = 3.8 \pm 0.9$. [5.42(15)] are consistent with $E2$ and $M2$ transitions, respectively. The larger relative errors in $\alpha_{264} = 0.77 \pm 0.24$ [0.106(2) for $E2$ and 0.205(6) for $M1$] and $\alpha_{287} = 0.88 \pm 0.73$ [0.365(12) for $E3$ and 0.689(19) for $M2$] did not allow a determination of the nature of these transitions. We note that the conversion coefficient analysis does not exclude an exchange of first 21^+ and 22^- assignments (as predicted by our calculations below) in Fig. 1. In this case, the presence of a ~1100-keV $24^- \rightarrow 22^-$ $E2$ transition may be expected in the γ-ray spectrum. However, no evidence for such a peak was found.

In Ref. [4], 12 γ rays were associated with the decay of the shorter lived isomeric state with $T_{1/2} = 42(5)$ ns. However, they were not placed in a level scheme. In the present work, 10 out of these transitions with energies of 128, 264, 287, 358, 725, 777, 855, 1184, 1258, and 1289 keV were detected as prompt γ rays in JUROGAM at the target position. Such a situation can be expected if transitions bypassing the isomer are present. The remaining two γ-rays with energies of 114.0 and 411.4 keV may well be originating directly from the decay of the shorter lived isomeric state and populating the 26^- and 27^+ states at energies of ~6164.8 and ~5867.4 keV, respectively. In this case, these transitions would be delayed and would be absent in the prompt γ-ray spectrum. These observations imply an excitation energy of $114.0 + 6164.8 = 411.0 + 5867.4 = 6278.8$ keV for the isomeric state that agrees well with ~6.3 MeV estimated in Ref. [4].

IV. DISCUSSION

Spin and parity assignments for the newly identified states above the 17^+ isomeric state in Fig. 1 were made through a comparison between data and calculations. In Ref. [4], calculations were performed with empirical two-body matrix elements (TBMEs) for protons in the $\pi 0h_{11/2}$ orbital. The TBMEs were obtained from the experimental levels of ^{148}Dy, which

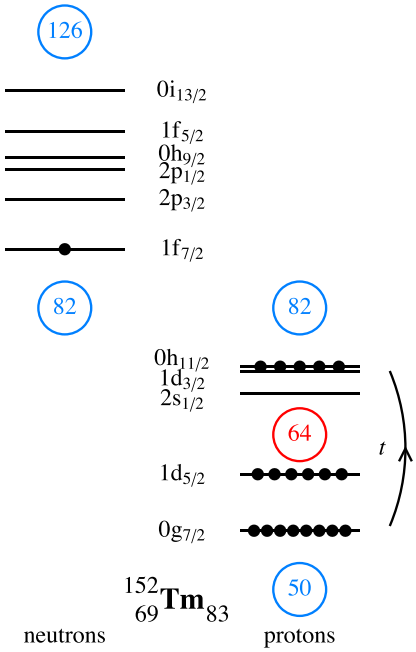

FIG. 7. The model space and the principle of the truncation as used in the large-scale shell-model calculation for ^{152}Tm. Shell closures are indicated in blue and the subshell closure at $Z = 64$ is shown in red. The number of protons excited across the $Z = 64$ subshell closure is denoted as t. As the $\pi 0h_{11/2}$ orbital is crucial for the description of high-spin states in ^{152}Tm, all five protons are schematically placed in this orbital.

has two valence protons outside the ^{146}Gd core, assuming a $Z = 64$ subshell closure [19]. No empirical TBMEs were available at that time (1986) for a proton in the $\pi 0h_{11/2}$ orbital and a neutron in the $\nu 1f_{7/2}$ orbital. Therefore, an interaction obtained from the global systematics of Schiffer and True [20] was used in Ref. [4]. The 17^+ isomeric state was found to have a $(\pi 0h_{11/2})^5 \nu 1f_{7/2}$ configuration with (proton-plus-neutron) seniority $\upsilon = 4$. In general, a good agreement with the levels of ^{152}Tm below the 17^+ isomeric state was found in Ref. [4]. However, the authors also commented that "significant improvements" would be possible if empirical TBMEs were also available for the proton-neutron interaction. In addition, the data obtained in this work for the levels above the isomeric state warranted new calculations. Here, we report on calculations in a large shell-model space in order to interpret the found levels and the known level scheme below the 17^+ isomeric state. The results are also interpreted in a simplified approach in a truncated valence space $(\pi 0h_{11/2})^5 \nu 1f_{7/2}$.

A. Large-scale shell model

The calculations in the large-scale shell-model space were performed with the codes ANTOINE [21] and KSHELL [22]. An inert ^{132}Sn core was assumed with valence protons and neutrons occupying orbitals in the 50–82 and 82–126 shells, respectively. The single-particle energies (see Fig. 7) were extracted from the properties (masses and level energies) of ^{132}Sn, ^{133}Sb, and ^{133}Sn, appropriate for the model space adopted in the full shell-model calculation. In particular, the single-proton energies of the $0g_{7/2}$, $1d_{5/2}$, $1d_{3/2}$, $2s_{1/2}$, and $0h_{11/2}$ orbitals were -9.667, -8.705, -6.959, -7.327, and -6.874 MeV, while the single-neutron energies of the $0h_{9/2}$, $1f_{7/2}$, $1f_{5/2}$, $2p_{3/2}$, $2p_{1/2}$, and $0i_{13/2}$ orbitals were -0.842, -2.403, -0.398, -1.549, -1.040, and 0.297 MeV, respectively. The realistic CWG Hamiltonian (a version of the interaction developed by Chou and Warburton [23]) was adopted, based on the charge-dependent (CD) Bonn force [24].

An estimate of the size of the model space can be obtained from the dimension formula for the antisymmetric representation $[1^N]$ of the Lie algebra U(Ω),

$$\dim[1^N] = \frac{\Omega!}{(\Omega - N)!N!}, \tag{1}$$

where Ω is the size of the single-particle space and N is the number of valence nucleons. In the case of ^{152}Tm, the numbers are $\Omega_\nu = 44$, $N_\nu = 1$ and $\Omega_\pi = 32$, $N_\pi = 19$, giving a dimension $d \approx 1.5 \times 10^{10}$. As the calculations are performed in the m scheme, this dimension is reduced by an order of magnitude, at the limit of the available computing power. Therefore, initially the strategy of Ref. [4] is adopted, where ^{152}Tm is treated as a ^{146}Gd core plus one valence neutron in the 82–126 shell and five valence protons in the 64–82 subshell, as shown in Fig. 7. In this lowest-order approximation, the dimension d is 3.5×10^5; in the m scheme, it further decreases and calculations can be easily carried out. To obtain a more realistic description of ^{152}Tm, a number of proton excitations, t, from the $(\pi 0g_{7/2}, \pi 1d_{5/2})$ into the $(\pi 1d_{3/2}, \pi 2s_{1/2}, \pi 0h_{11/2})$ orbitals are allowed. A calculation with unrestricted t, which includes all proton configurations in the 50–82 shell, shall be referred to as the "full" shell-model calculation. In all cases, the entire 82–126 shell is taken without any truncation for the one neutron outside the $N = 82$ shell closure.

States with all possible angular momenta J are obtained in a model space with angular-momentum projection of $M = 0$. With the available computing resources, this can be done for the case where two proton excitations across the $Z = 64$ subshell are allowed, i.e., for $t \leqslant 2$. With this truncation, the lowest eigenstate has $J^\pi = 9^+$, closely followed by a $J^\pi = 8^+$ level. In addition, the positive-parity levels of interest in the experimental spectrum have $J \geqslant 8$. Therefore, it is reasonable to use a model space with $M = 8$. This is advantageous because the dimension d decreases with increasing M and calculations can be performed in the full shell-model space for $M = 8$. Similarly, a model space with $M = 11$ is sufficient to study the features of the negative-parity level structure.

The energy spectra of the nucleus ^{152}Tm calculated in the full shell-model space (LSSM) are compared with the observed levels (Expt) in Fig. 8. The experimental and calculated energies of the yrast 9^+ state are both set to zero and all other energies are shown relative to this level. The observed 9^+-11^+-13^+-15^+-17^+-19^+-21^+ sequence is well reproduced in the calculation (with a mean-square energy deviation of $\Delta E = 0.214$ MeV) and therefore can be fixed with reasonable confidence. The 16^+ level is calculated to be at an excitation energy of 2.769 MeV, more than 300 keV above the 17^+ isomer. The observed 8^+-9_2^+-10^+-11^--12^--13^--15^--18^--20^--22^- sequence is also present in the calculation. Although the order of the levels

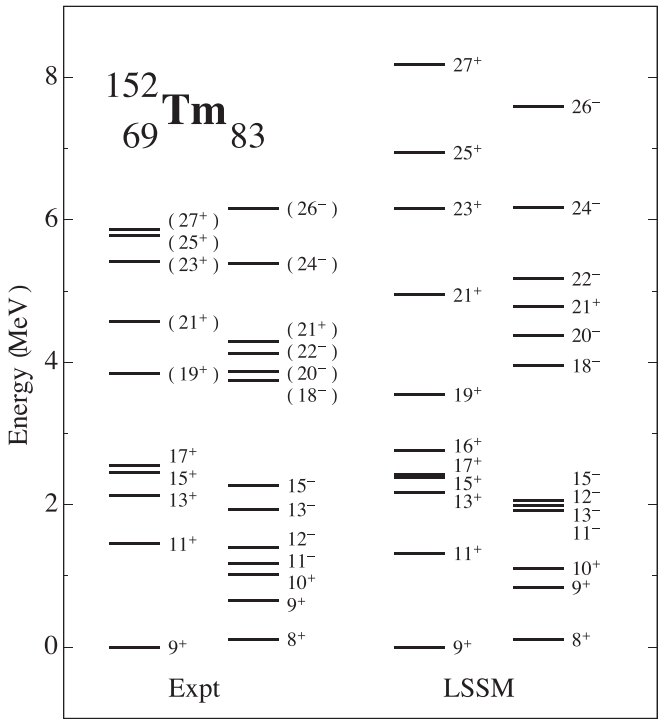

FIG. 8. The observed spectrum of the nucleus ^{152}Tm (Expt) compared with the results of the full large-scale shell-model (LSSM) calculation. The energy of the 9^+ level is set to zero.

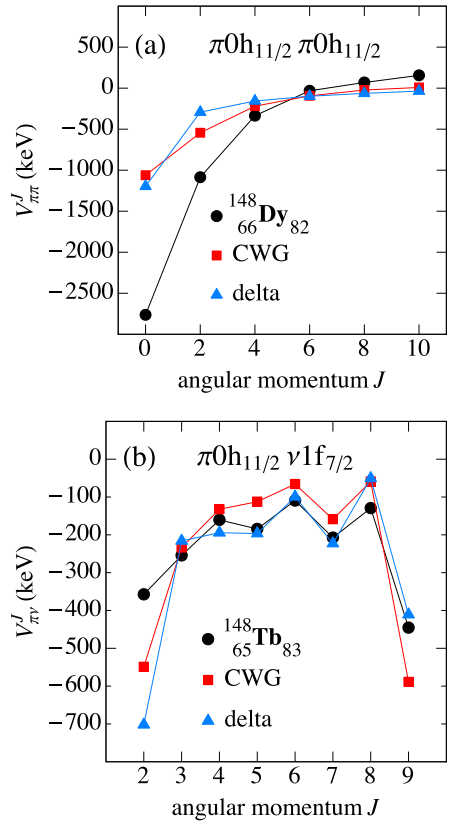

FIG. 9. Two-body matrix elements $V^J_{\pi\nu}$ as a function of the coupled angular momentum J for (a) two protons in the $\pi 0h_{11/2}$ orbital and (b) a proton in the $\pi 0h_{11/2}$ orbital and a neutron in the $\nu 1f_{7/2}$ orbital. The empirical matrix elements (black circles) are shifted so that their monopole average coincides with that of the CWG matrix elements (red squares). The blue triangles correspond to a δ interaction with the same monopole average.

is almost correct, the agreement is less satisfactory for the negative-parity levels, with a mean-square energy deviation of $\Delta E = 0.581$ MeV. In particular, the 11^--12^--13^--15^- multiplet is too compressed in the calculation. This points to a possible deficiency of the interaction but we have chosen not to modify the TBMEs of Ref. [24]. Alternatively, it could be due to a much restricted valence space for the negative-parity states. As to the $J > 21$ levels, the discrepancies in energy increase with increasing angular momentum and become very large for $J \sim 27$. Therefore, it is possible that the states with $J > 21$ have a structure that is beyond the scope of the current model space.

B. Simplified shell model

Effective single-particle energies (ESPEs) change with nucleon number due to the monopole components of the nucleon-nucleon interaction. Therefore, the ordering and evolution of ESPEs across a region of nuclei under consideration is model specific. To achieve further insight into the observed levels in ^{152}Tm, a simplified model is considered, appropriate for the region around ^{146}Gd. In particular, a model space with five protons in the $\pi 0h_{11/2}$ orbital and one neutron in the $\nu 1f_{7/2}$ orbital may provide a simplified description of the high-spin positive-parity levels in ^{152}Tm. This simplified model is based on two observations: (i) the first-excited $13/2^+$ level is ~1 MeV above the $7/2^-$ ground state in ^{147}Gd and (ii) the $11/2^-$ level is the lowest in energy with negative parity in ^{147}Tb. To perform calculations in this model space, the TBMEs for protons in the $\pi 0h_{11/2}$ orbital as well as those between a proton in the $\pi 0h_{11/2}$ orbital and a neutron in the $\nu 1f_{7/2}$ orbital are required. Such empirical interactions can be extracted from the spectra of ^{148}Dy and ^{148}Tb, respectively.

A comparison of the empirical matrix elements with the corresponding ones of the CWG Hamiltonian is presented in Fig. 9. The empirical matrix elements are shifted in order to have the same monopole average as that of the CWG matrix elements. A striking difference occurs for the pairing ($J = 0$) matrix element between the protons. The pairing correlations in several orbitals are naturally built into the CWG Hamiltonian. To simulate such correlations in a single-orbital calculation, a strongly attractive pairing matrix element is needed. Therefore, the empirical pairing matrix element is much more attractive compared to the one from the CWG Hamiltonian. To a lesser extent, the same comment is valid for the quadrupole pairing ($J = 2$) matrix element between the protons. The empirical and CWG proton-neutron matrix elements display a consistent behavior as a function of the coupled angular momentum J. In these comparisons, it should not be forgotten that the empirical and microscopic interactions are tailored for different model spaces and therefore differences can be expected. Figure 9 also shows the matrix elements as obtained with a δ interaction, with

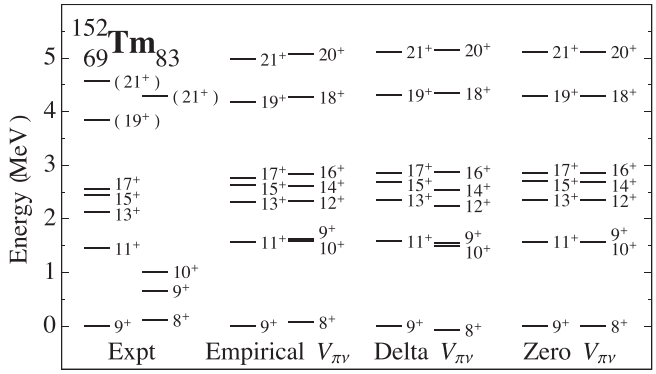

FIG. 10. The observed positive-parity spectrum of ^{152}Tm (Expt) compared to the results of three different calculations with empirical, δ, and zero proton-neutron interactions in the $(\pi 0h_{11/2})^5 \nu 1f_{7/2}$ model space (see the text for details).

a strength adjusted such that its monopole average coincides with that of the CWG matrix elements.

Figure 10 shows the energy spectra resulting from three different simplified shell-model calculations: (i) with empirical proton-neutron matrix elements, (ii) with proton-neutron matrix elements from a δ interaction, and (iii) with zero proton-neutron interaction. In all calculations, the empirical proton-proton interaction is taken since both the CWG and the δ proton-proton TBMEs lead to poor results if employed in a restricted model space. For example, the excitation energy of the 17^+ level with respect to the yrast 9^+ state is calculated using CWG to be less than half the observed energy. This discrepancy is caused by the above-mentioned differences in the pairing matrix elements. The calculation with the empirical proton-neutron matrix elements correctly predicts $J^\pi = 9^+$ for the ground state. This angular momentum is favored by two effects. First, the proton-neutron matrix element for $J = 9$ is strong and attractive (see Fig. 9). Second, the number of $(\pi 0h_{11/2})^5 \nu 1f_{7/2}$ states is close to the maximum for $J = 9$, namely 30, and as a result correlations bring down the 9_1^+ level in energy. There are slightly more states (33) for $J = 6$ and 7. However, due to the weak proton-neutron interaction for these angular momenta (see Fig. 9), the 6_1^+ and 7_1^+ levels occur at higher energies as compared to that of the 9_1^+ state.

The yrast 9^+-11^+-13^+-15^+-17^+-19^+-21^+ sequence is correctly reproduced in the simplified shell model, irrespective of the proton-neutron interaction that is used in the calculation. The results up to the 17^+ isomeric state are close to those obtained by McNeill *et al.* [4], presumably because of the closeness of proton-neutron interaction ($V_{\pi\nu}$) estimated from systematics to the present one obtained from data. It is seen from Fig. 10 that the proton-neutron interaction has some influence on the energy spectrum; namely, it lifts the degeneracy of certain levels. For example, the 8_1^+ and 9_1^+ levels are degenerate in the absence of a proton-neutron interaction and the observed splitting of these levels (114 keV) illustrates the expected energy shifts due to the $V_{\pi\nu}$ matrix element. If one assumes that both the states originate from a five-proton configuration with seniority $\upsilon_\pi = 1$, the difference in their energies can be written as

$$
\begin{aligned}
&E(8_1^+) - E(9_1^+) \\
&\quad = \frac{3}{11}V_{\pi\nu}^2 + \frac{21}{715}V_{\pi\nu}^3 - \frac{81}{715}V_{\pi\nu}^4 - \frac{51}{455}V_{\pi\nu}^5 - \frac{87}{1540}V_{\pi\nu}^6 \\
&\qquad - \frac{1161}{68068}V_{\pi\nu}^7 + \frac{11953}{20020}V_{\pi\nu}^8 - \frac{2653}{4420}V_{\pi\nu}^9, \qquad (2)
\end{aligned}
$$

where $V_{\pi\nu}^J$ is the TBME between a proton in the $\pi 0h_{11/2}$ orbital and a neutron in the $\nu 1f_{7/2}$ orbital coupled to angular momentum J. This result is obtained with use of Eq. (1) of Ref. [25]. As the coefficients in the expansion (2) sum to zero, the two levels are degenerate for a $V_{\pi\nu}^J$ that is constant with J. The coefficients in front of $V_{\pi\nu}^J$ are small except for $J = 2, 8, 9$ and, furthermore, $V_{\pi\nu}^8$ is small (see Fig. 9). Therefore, the energy difference $E(8_1^+) - E(9_1^+)$ results mainly from $V_{\pi\nu}^J$ in the antialigned ($J = 2$) and the aligned ($J = 9$) configurations, and it is seen from Eq. (2) that their effects are opposite. This provides a qualitative explanation of the observed near degeneracy of the two levels.

The energies of the 9_2^+ and 10_1^+ levels are not reproduced by the simplified shell model. This can be understood using the results of the full shell model, where these states have a dominant component (>90%) with the neutron in the $\nu 0h_{9/2}$ orbital instead of the $\nu 1f_{7/2}$ orbital. Therefore, the splitting of the 9_2^+ and 10_1^+ levels is mainly due to the $\pi 0h_{11/2}$–$\nu 0h_{9/2}$ interaction. One can again make a qualitative estimate of the energy difference, following Ref. [25], by assuming that the five-proton configuration has seniority $\upsilon_\pi = 1$, leading to the expression

$$
\begin{aligned}
&E(10_1^+) - E(9_2^+) \\
&\quad = -\frac{2}{11}V_{\pi\nu}^1 - \frac{50}{429}V_{\pi\nu}^2 + \frac{8}{429}V_{\pi\nu}^3 + \frac{72}{715}V_{\pi\nu}^4 \\
&\qquad + \frac{19}{195}V_{\pi\nu}^5 + \frac{31}{561}V_{\pi\nu}^6 + \frac{50}{2431}V_{\pi\nu}^7 \\
&\qquad + \frac{122}{24453}V_{\pi\nu}^8 - \frac{65558}{109395}V_{\pi\nu}^9 + \frac{12598}{20995}V_{\pi\nu}^{10}, \qquad (3)
\end{aligned}
$$

where $V_{\pi\nu}^J$ is now the TBME between a proton in the $\pi 0h_{11/2}$ orbital and a neutron in the $\nu 0h_{9/2}$ orbital. A similar analysis as that discussed above leads to the conclusion that the energy difference $E(10_1^+) - E(9_2^+)$ results mainly from the proton-neutron interaction in the $J = 1, 2$ and the $J = 10$ configurations, which are seen to have opposite effects. For the $\pi 0h_{11/2}$ and $\nu 0h_{9/2}$ orbitals the former TBMEs are strongly attractive (in particular for $J = 1$) while the latter are less so, which constitutes a qualitative explanation of the larger observed energy splitting (361 keV) in this case.

A final remark of this section concerns the large energy spacing between the 19^+ and 17^+ levels. In the simplified shell model, it results from a change in structure for the protons, from proton seniority $\upsilon_\pi = 3$ to $\upsilon_\pi = 5$ (which corresponds to proton-plus-neutron seniority $\upsilon = 4$ to $\upsilon = 6$). This is in line with the explanation advocated in Ref. [4].

TABLE III. The coefficients P_J and N_J in Eq. (4) of transitions in the yrast sequence 9^+-21^+ in ^{152}Tm for different choices of the proton-neutron interaction in the simplified shell model, and in the full large-scale shell model (LSSM).

	(P_J, N_J)			
$J_i^\pi \to J_f^\pi$	Empirical	δ	Zero	LSSM
$11^+ \to 9^+$	(2.37,0.04)	(2.35,0.05)	(2.36,0)	(3.78,0.51)
$13^+ \to 11^+$	(0.99,0.03)	(1.14,0.03)	(0.62,0)	(2.34,0.44)
$15^+ \to 13^+$	(0.64,0.04)	(0.81,0.02)	(0.62,0)	(2.23,0.63)
$17^+ \to 15^+$	(0.05,0.03)	(0.24,0.12)	(0.40,0)	(2.01,0.63)
$19^+ \to 17^+$	(1.97,0.02)	(1.97,0.02)	(1.97,0)	(2.57,0.36)
$21^+ \to 19^+$	(1.71,0.03)	(1.71,0.03)	(1.71,0)	(0.11,0.00)

C. Electric quadrupole transition rates

The $B(E2)$ values of transitions in the yrast sequence 9^+-21^+ can be expressed as

$$B(E2; J \to J-2) = (P_J e_\pi + N_J e_\nu)^2 b^4. \quad (4)$$

Here, e_π and e_ν are the effective charges of the proton and neutron, respectively, b is the length parameter of the harmonic oscillator, and P_J and N_J are numerical constants, listed in Table III for the simplified shell model with various proton-neutron interactions and in the full large-scale shell model. One observes that the $E2$ transitions are dominated by the protons, except for the $17^+ \to 15^+$ transition, for which the contributions of the protons and the neutron can become comparable. In the simplified shell model, the isomerism of the 17^+ level is therefore explained by the fact that $E2$ transitions with $\Delta\upsilon = 0$ are suppressed if the number of protons in the $\pi 0h_{11/2}$ orbital is close to six (midshell). This feature is lost, however, in the large-scale shell-model calculation where the decrease of the proton $E2$ matrix element from 11^+ to 17^+ is much less pronounced. Seniority mixing may be at the basis of this feature since it may lead to a stronger contribution of $E2$ transitions with $\Delta\upsilon = 2$, which, in contrast to those with $\Delta\upsilon = 0$, peak at midshell.

Table IV lists the corresponding $B(E2)$ values, calculated with standard effective charges, $e_\pi = 1.5e$ for the proton and $e_\nu = 0.5e$ for the neutron, and with the oscillator length $b = 2.31$ fm. A single experimental value is known from the decay of the isomeric state [4] and is of the order of a single-particle transition, i.e., one Wu, which is 48.19 e^2 fm^4 in ^{152}Tm. It is seen that the $B(E2; 17^+ \to 15^+)$ value depends sensitively on the proton-neutron interaction and varies over more than an order of magnitude. Table IV also lists the $B(E2)$ values in the 50–82 model space for the protons, calculated in the full large-scale shell model. In this approximation, the yrast 9^+-19^+ sequence is connected with strong $E2$ transitions, indicating the increased collectivity in the large model space but this decay pattern breaks down at $J^\pi = 21^+$. In the case of the isomeric $17^+ \to 15^+$ transition, the calculated $B(E2)$ value is larger by an order of magnitude in the large-scale shell model compared to the data, probably due to an overestimation of the mixing of configurations.

TABLE IV. The $B(E2; J_i^\pi \to J_f^\pi)$ values of transitions in the yrast sequence 9^+-21^+ in ^{152}Tm for different choices of the proton-neutron interaction in the simplified shell model, and in the full large-scale shell model (LSSM).

	$B(E2; J_i^\pi \to J_f^\pi)$ (e^2 fm^4)				
$J_i^\pi \to J_f^\pi$	Empirical	δ	Zero	LSSM	Expt
$11^+ \to 9^+$	363	359	357	1015	
$13^+ \to 11^+$	63	85	25	405	
$15^+ \to 13^+$	27	42	25	388	
$17^+ \to 15^+$	0.21	5.2	10	321	44 (2)
$19^+ \to 17^+$	251	251	249	473	
$21^+ \to 19^+$	189	189	187	1	

An important feature of ^{146}Gd is the presence of the 3^- state as its lowest excited state with a $B(E3)$, revealing that it is indeed an octupole vibrational state. This octupole excitation is seen in low-lying excitations of many nuclei in this region. In ^{152}Tm, the 11^- state was interpreted to be arising from the $9^+ \times 3^-$ configuration [4]. The large-scale shell-model calculation has difficulty in reproducing the observed negative-parity states in ^{152}Tm, indicating that insufficient octupole correlations are present in the calculation.

V. SUMMARY

A level scheme above the known 17^+ isomeric state in the odd-odd nucleus ^{152}Tm was established. Results of our large-scale shell-model calculations were presented for the high-spin states, assuming an inert ^{132}Sn core. The yrast sequence of the levels up to the 21^+ state could also be satisfactorily interpreted with this approach. Most of the positive-parity states were well explained in a simplified approach, in a model space of $(\pi 0h_{11/2})^5 \nu 1f_{7/2}$ configurations. The structure of the states with $J \geqslant 23$ could not be explained, possibly due to the limitations of the model space. The predicted quadrupole transition rates from large-scale shell-model calculations were mostly consistent with the relative intensities of the observed γ rays, especially those corresponding to the $E2$ transitions. Future measurements of the lifetime of levels residing below as well as above the isomeric state would provide further insight into the influence of the proton-neutron interaction on the level structures in this nucleus.

ACKNOWLEDGMENTS

This work was supported by the EU 7th Framework Programme, Integrating Activities Transnational Access, Project No. 262010 ENSAR, and by the Academy of Finland under the Finnish Centre of Excellence Programme (Nuclear and Accelerator Based Physics Programme at JYFL). The authors acknowledge GAMMAPOOL support for the JUROGAM detectors and B.S.N.S., D.M.C., M.J.T., S. K., and D.D. acknowledge the support of the Science and Technology Facilities Council, Grant No. ST/L005794/1. M.V. acknowledges the support of the Slovak Research and Development Agency under Contract No. APVV-15-0225 and the Slovak Grant Agency VEGA (Contract No. 2/0129/17). The theoretical work was supported by the Sandwich PhD scholarship programme 2008-09 from Embassy of France in India.

[1] P. Kleinheinz, R. Broda, P. J. Daly, S. Lunardi, M. Ogawa, and J. Blomqvist, Z. Phys. A **290**, 279 (1979).
[2] R. D. Lawson, Z. Phys. A **303**, 51 (1981).
[3] L. K. Peker, E. I. Volmyansky, V. E. Bunakov, and S. G. Ogloblin, Phys. Lett. B **36**, 547 (1971).
[4] J. McNeill, R. Broda, Y. H. Chung, P. J. Daly, Z. W. Grabowski, H. Helppi, M. Kortelahti, R. V. F. Janssens, T. L. Khoo, R. D. Lawson *et al.*, Z. Phys. A **325**, 27 (1986).
[5] Y. H. Chung, P. J. Daly, H. Helppi, R. Broda, Z. W. Grabowski, M. Kortelahti, J. McNeill, A. Pakkanen, P. Chowdhury, R. V. F. Janssens *et al.*, Phys. Rev. C **29**, 2153 (1984).
[6] E. Ideguchi, Y. Gono, S. Mitarai, T. Morikawa, A. Odahara, M. Kidera, M. Sibata, H. Tsuchida, K. Miyazaki, M. Oshima *et al.*, Z. Phys. A **352**, 363 (1995).
[7] T. Bhattacharjee, D. Banerjee, S. K. Das, S. Chanda, T. Malik, A. Chowdhury, P. Das, S. Bhattacharyya, and R. Guin, Phys. Rev. C **88**, 014313 (2013).
[8] B. Cederwall, F. Ghazi Moradi, T. Bäck, A. Johnson, J. Blomqvist, E. Clément, G. de France, R. Wadsworth, K. Andgren, K. Lagergren *et al.*, Nature (London) **469**, 68 (2011).
[9] K. Ogawa, Phys. Rev. C **28**, 958(R) (1983).
[10] B. S. Nara Singh, Z. Liu, R. Wadsworth, H. Grawe, T. S. Brock, P. Boutachkov, N. Braun, A. Blazhev, M. Górska, S. Pietri *et al.*, Phys. Rev. Lett. **107**, 172502 (2011).
[11] P. J. Nolan, F. A. Beck, and D. B. Fossan, Annu. Rev. Nucl. Part. Sci. **45**, 561 (1994).
[12] M. Leino, J. Äystö, T. Enqvist, P. Heikkinen, A. Jokinen, M. Nurmia, A. Ostrowski, W. H. Trzaska, J. Uusitalo, K. Eskola *et al.*, Nucl. Instrum. Methods Phys. Res., Sect. B **99**, 653 (1995).
[13] J. Sarén, J. Uusitalo, M. Leino, and J. Sorri, Nucl. Instrum. Methods Phys. Res., Sect. A **654**, 508 (2011).
[14] R. D. Page, A. N. Andreyev, D. E. Appelbe, P. A. Butler, S. J. Freeman, P. T. Greenlees, R.-D. Herzberg, D. G. Jenkins, G. D. Jones, P. Jones *et al.*, Nucl. Instrum. Methods Phys. Res., Sect. B **204**, 634 (2003).
[15] I. H. Lazarus, D. E. Appelbe, P. A. Butler, P. J. Coleman-Smith, J. R. Cresswell, S. J. Freeman, R. D. Herzberg, I. Hibbert, D. T. Joss, S. C. Letts *et al.*, IEEE Trans. Nucl. Sci. **48**, 567 (2001).
[16] P. Rahkila, Nucl. Instrum. Methods **595**, 637 (2008).
[17] D. C. Radford, Nucl. Instrum. Methods **361**, 297 (1995).
[18] T. Kibédi, T. W. Burrows, M. B. Trzhaskovskaya, P. M. Davidson, and C. W. Nestor Jr., Nucl. Instrum. Methods A **589**, 202 (2008).
[19] P. J. Daly, P. Kleinheinz, R. Broda, S. Lunardi, H. Backe, and J. Blomqvist, Z. Phys. A **298**, 173 (1980).
[20] J. P. Schiffer and W. W. True, Rev. Mod. Phys. **48**, 191 (1976).
[21] E. Caurier and F. Nowacki, Acta Phys. Pol. B **30**, 705 (1999).
[22] N. Shimizu, KSHELL code, arXiv:1310.5431 [nucl-th] (unpublished).
[23] W. T. Chou and E. K. Warburton, Phys. Rev. C **45**, 1720 (1992).
[24] B. A. Brown, N. J. Stone, J. R. Stone, I. S. Towner, and M. Hjorth-Jensen, Phys. Rev. C **71**, 044317 (2005).
[25] M. Rejmund, A. Navin, S. Biswas, A. Lemasson, M. Caamaño, E. Clément, O. Delaune, F. Farget, G. de France, B. Jacquot *et al.*, Phys. Lett. B **753**, 86 (2016).